Received: 31 May 2019 | Revised: 1 August 2019 | Accepted: 6 August 2019

DOI: 10.1002/jbm.b.34477

ORIGINAL RESEARCH REPORT

Society For Biomaterials WILEY

Biocompatibility of (Ba,Ca)(Zr,Ti)O_3 piezoelectric ceramics for bone replacement materials

Kara K. Poon[1] | Matthias C. Wurm[2] | Donald M. Evans[1] | Mari-Ann Einarsrud[1] | Rainer Lutz[2] | Julia Glaum[1]

[1]Department of Materials Science and Engineering, NTNU Norwegian University of Science and Technology, Trondheim, Norway

[2]Department of Oral and Maxillofacial Surgery, Friedrich-Alexander-Universität Erlangen-Nürnberg, Erlangen, Germany

Correspondence
Kara K. Poon, Kjemi 2-332, Gløshaugen, Sem Sælands vei 12, 7491, Trondheim, Norway.
Email: kara.poon@ntnu.no

Funding information
H2020 Marie Skłodowska-Curie Actions, Grant/Award Number: H2020- MSCA-IF-2014 Grant 655866; Norges Forskningsråd, Grant/Award Number: FRINATEK Project 250098

Abstract

Total joint replacement implants are generally designed to physically mimic the biological environment to ensure compatibility with the host tissue. However, implant instability exposes patients to long recovery periods, high risk for revision surgeries, and high expenses. Introducing electrical stimulation to the implant site to accelerate healing is promising, but the cumbersome nature of wired devices is detrimental to the implant design. We propose a novel strategy to stimulate cells at the implant site by utilizing piezoelectric ceramics as electrical stimulation sources. The inherent ability of these materials to form electric surface potentials under mechanical load allows them to act as internal power sources. This characteristic is commonly exploited in non-biomedical applications such as transducers or sensors. We investigate calcium/zirconium-doped barium titanate (BCZT) ceramics in an *in vitro* environment to determine their potential as implant materials. BCZT exhibits low cytotoxicity with human osteoblast and endothelial cells as well as high piezoelectric responses. Microstructural adaptation was identified as a route for optimizing piezoelectric behavior. Our results show that BCZT is a promising system for biomedical applications. Its characteristic ability to autonomously generate electric surface potentials opens the possibility to functionalize existing bone replacement implant designs to improve implant ingrowth and long-term stability.

KEYWORDS
BCZT, cell proliferation and cytotoxicity, endothelial cells, osteoblasts, piezoelectric ceramics

1 | INTRODUCTION

Bone regenerative therapies involving the replacement or augmentation of diseased, or injured, bone tissue with implants are a standard procedure in current clinical practice. Today, synthetic bone replacement materials such as ceramics, metals, polymers, and glasses physically mimic the biological environment to ensure compatibility between the living tissue and the implant (Saini, Singh, Arora, Arora, & Jain, 2015). Strength, stiffness, topography, and toughness are the most carefully considered properties in implant design (Mandracci, Mussano, Rivolo, & Carossa, 2016; Smeets et al., 2016; Vandrovcová & Bačáková, 2011). Recent advancements in tissue engineering have focused on the use of biochemical and physicochemical cues to trigger specific cell responses to encourage better biological interaction between the implant and the living tissue.

A novel approach to improve the interface between synthetic materials and living bone tissue is to elicit particular cell behaviors with mechanical and electrical stimulation. The cell response to mechanical stimulation is well described by Wolff's law (Wolff, 1892), which states that the inner architecture of bone will adapt and restructure itself to withstand the mechanical forces acting upon it. In addition, cells convert mechanical stimuli into electrochemical activity via a number of mechanisms classified under the general term of "mechanotransduction" (Orr, Helmke, Blackman, & Schwartz, 2006). One of these mechanisms is the formation of electric potentials in load-bearing bone upon application of mechanical stress (Rajabi, Jaffe, & Arinzeh, 2015; Riddle & Donahue, 2009). *In vivo* studies indicate that direct current electrical stimulation applied to an implant site enhances initial-stage implant osseointegration, improves interfacial strength, and increases bone formation (Dergin et al., 2013; Isaacson et al., 2011; Salman & Park, 1980). In current clinical practice, electrical stimulation is used to treat non-union fractures via direct current, inductive, and capacitive coupling procedures (Aleem et al., 2016; Griffin & Bayat, 2011; Kuzyk & Schemitsch, 2009). These procedures rely on an external power source and the electrical stimulation can only be applied infrequently. For constant and power source independent electrical stimulation of the bone tissue, it is thus crucial to develop implant materials that autonomously generate electric charges under mechanical loads as they are generated by the body itself.

Piezoelectric ceramics may be the key to functionalizing current implant designs, as they exhibit mechanically generated electric surface potentials due to their non-centrosymmetric crystal structure. Thus, they can be used to mimic the bone's ability to generate electrical potentials under a mechanical load without the need for an external power source. Piezoelectric ceramics as bone replacement materials are currently not used in implant devices; however, *in vitro* studies indicate improved biocompatibility and bone-inductive ability on piezoelectric ceramic surfaces (Bodhak, Bose, & Bandyopadhyay, 2009; Tofail & Bauer, 2016).

A piezoelectric ceramic to be used as an active bone replacement material should be biocompatible and induce a sufficiently high electric potential to stimulate human cells (Büchter et al., 2005; Foulds & Barker, 1983; Hartig, Joos, & Wiesmann, 2000; Kuzyk & Schemitsch, 2009; Meyer, Büchter, Wiesmann, Joos, & Jones, 2005; Minary-Jolandan & Yu, 2009; Wiesmann, Hartig, Stratmann, Meyer, & Joos, 2001; Zigman et al., 2013). The highest piezoelectric coefficients, which quantify the generation of charge per unit of mechanical load, are currently achieved by lead-based piezoelectric ceramics; however, their high lead content renders them toxic (Shrout & Zhang, 2007). Among the lead-free piezoelectric systems, barium titanate (BT)-based materials are a promising class for bone replacement as indicated by cytotoxicity, cell viability, and proliferation studies (Ball, Mound, Nino, & Allen, 2014; Baxter, Bowen, Turner, & Dent, 2010; Park et al., 1981; Tang et al., 2017; Zhang, Chen, Zeng, Zhou, & Zhang, 2014). Particularly, the BT-derivative (Ba,Ca)(Zr,Ti)O_3 (BCZT) is of interest because of exceptionally high piezoelectric values compared to other lead-free piezoelectric materials available today (Liu & Ren, 2009). Additionally, fracture analysis studies of BCZT indicate that the hardness values of BCZT are approximately one to two orders of magnitude larger than human bone tissue, and approximately of the same order of magnitude for fracture toughness (Esguerra-Arce et al., 2015; Lucksanasombool, Higgs, Higgs, & Swain, 2001; Öhman, Zwierzak, Baleani, & Viceconti, 2013; Phelps, Hubbard, Wang, & Agrawal, 2000; Prabahar et al., 2017; Rattanachan, Miyashita, & Mutoh, 2005; Sailaja et al., 2019; Srinivas et al., 2015; Zioupos & Currey, 1998).

In this study, we investigate the piezoelectric properties of $(Ba_{0.85}Ca_{0.15})(Zr_{0.10}Ti_{0.90})O_3$ bulk ceramics and their compatibility with primary human osteoblast cells (HOBs) and primary human umbilical vein endothelial cells (HUVECs). The piezoelectric performance of the BCZT ceramics was determined as two orders of magnitude larger than observed in type I collagen fibrils, which are one of the origins of the stress-induced electric potentials in bone (Minary-Jolandan & Yu, 2009). In addition, the ceramic's piezoelectric response depends on the grain size, highlighting the possibility to tune the piezoelectric characteristics through microstructural modifications. Cytotoxicity, cell proliferation, and cell viability studies were performed using HOB and HUVEC cells. These cell studies demonstrate low cytotoxicity and enhanced cell viability and proliferation on the BCZT ceramics as compared to a polystyrene control group. The combination of good piezoelectric performance and low cytotoxicity highlights the potential of this class of materials to mimic the "piezoelectric effect" observed in natural bone, making it suitable for active, cell stimulating implants.

2 | MATERIALS AND METHODS

$(Ba_{0.85}Ca_{0.15})(Zr_{0.10}Ti_{0.90})O_3$ (BCZT) ceramics were synthesized via a solid-state reaction following the procedure by Zhang et al. (2014). This BCZT composition was chosen as it is located at the morphotropic phase boundary (MPB), where a high piezoelectric coefficient can be expected (Bai et al., 2015; Zhang, Glaum et al., 2014). The synthesis procedures of BCZT Series 1 and Series 2 were identical, only the barium carbonate precursor powder was of different purity (≥ 99% (Sigma Aldrich) for Series 1 and ≥99.98% (Sigma Aldrich) for Series 2). The other precursor powders were calcium carbonate ($CaCO_3$ ≥99%, Sigma Aldrich), zirconium dioxide (ZrO_2 ≥99.978%, Alfa Aesar), and titanium dioxide (TiO_2 ≥99.8%, Sigma Aldrich). The precursor powders were ball-milled in a 250 mL HDPE milling bottle on a long roll jar mill (U.S. Stoneware, East Palestine) for 24 hr with 5 mm diameter yttria-stabilized zirconia milling balls (Tosoh, Amsterdam, Netherlands) in 96% ethanol. The mixed precursor powders were dried using a rotary evaporator (Büchi Labortechnik AG, Flawil, Switzerland) and sieved using a 250 μm mesh. Subsequently, the powders were uniaxially pressed into cylindrical discs (3 g, 25 mm in diameter). The pellets were calcined at 1300°C for 2 hr, with a heating rate of 350°C/hr and a cooling rate of 400°C/hr. After calcination, the pellets were ground using an agate mortar and pestle, sieved with a 250 μm mesh, ball-milled in ethanol for 24 hr, and dried using a rotary evaporator. Calcined powders were sieved with a 250 μm mesh and uniaxially pressed into cylindrical disks (0.5 g, 15 mm in diameter). The green body pellets were sintered at

1450°C for 3 hr, with a heating rate of 350°C/hr and a cooling rate of 400°C/hr. Platinum crucibles were used for both calcination and sintering to avoid chemical reactions between the samples and the crucibles. Sintered pellets were approximately 12 mm in diameter and 1 mm in thickness. In total, 88 pellets of BCZT Series 1 were produced, as well as 23 pellets of BCZT Series 2. The bulk density of the sintered BCZT samples was determined from geometric measurements using a digital caliper and is presented as mean and *SD*.

Plan view images of the grain microstructure and surface topography of the BCZT and polystyrene control group materials used in the cell testing were obtained using a Zeiss Ultra 55 scanning electron microscope (SEM) (Carl Zeiss AG, Oberkochen, Germany). To expose the grain boundaries, BCZT samples were polished to a 3 μm finish, chemically etched using 37% hydrochloric acid and deionized water in a 1:1 ratio for 30 s (≈ 6.1 M), thermally etched at 1350°C for 5 min using a heating and cooling rate of 600°C/hr, and carbon coated prior to imaging. For cell testing, BCZT samples were grinded using 1200 grit silicon carbide (SiC) paper, whereas polystyrene samples (T175 Nunc™ EasYFlask™, Thermo Scientific, Waltham, MA) were used as-received.

Grain size measurements were performed using Lince software (Lince 2.31, Ceramics Group, TU Darmstadt, Germany), following a linear intercept method. At least 50 intersections were measured for each series of BCZT and expressed as mean and *SD*.

The phase purity of the BCZT ceramics was determined by X-ray diffraction (XRD) on sintered samples ground into powders with an agate mortar and pestle. A Bruker D8 A25 DaVinci X-ray diffractometer (Bruker, Billerica, MA) with an accelerating Cu Kα radiation of 1.54 Å was used. Phase purity analysis was performed with respect to PDF 00-065-0109 (International Center for Diffraction Data, Newtown Square, PA, 2016).

In preparation for piezoelectric property measurements, samples were grinded using 1200 grit SiC paper, and gold electrodes were applied by sputter deposition. Piezoelectric coefficient, d_{33}, measurements were performed using a TF Analyzer 2000 (aixACCT Systems GmbH, Aachen, Germany). The piezoelectric coefficient was measured using a small signal frequency and amplitude of 1 kHz and 3 V, respectively. At least five measurements were performed on one sample of each series and are expressed as mean and *SD*.

Surface property measurements were performed on BCZT samples grinded using 1200 grit SiC paper and as-received polystyrene samples, prepared as for the cell tests. The surface roughness was determined using an NT-MDT Ntegra Prima Scanning Probe Microscope (NT-MDT Spectrum Instruments Ltd., Moscow, Russia) with HQ:NSC35/Pt tips in contact mode. The scan size area was 85 × 85 μm^2. The static contact angles of sessile drops of 1 μL deionized water on BCZT and polystyrene samples were measured using the Krüss Drop Shape Analyzer DSA100 (Krüss GmbH, Hamburg, Germany). Deionized water drops were deposited at a speed of 40 mm/min and were allowed to sit on the sample surface for 30 s before the measurement was taken. Ten independent measurements per sample were obtained at 37°C. The contact angles were determined using the Young-Laplace fitting method. They are presented as mean and *SD*.

Cell viability and proliferation tests were performed on BCZT samples, which were grinded using 1200 grit SiC paper, and on as-received polystyrene samples of 12 mm diameter (Wurm et al., 2017). Primary human umbilical vein endothelial cells (HUVEC, PromoCell GmbH, Heidelberg, Germany) and primary human osteoblast cells (HOB, PromoCell GmbH, Heidelberg, Germany) were used for cell testing. The cells were cultured in flasks with cell growth areas of 25, 75, and 175 cm^2 (Greiner Bio-One, Frickenhausen, Germany) with Endothelial Cell Growth Medium (Ready-to use) (PromoCell GmbH, Heidelberg, Germany) at 98% humidity, 37°C, and 5% CO_2 (Heracell 240i CO_2 incubator, Thermo Scientific, Waltham, MA). At 70–90% confluency, splitting was performed until the third passage. A 24-well plate was filled with the corresponding media, and a 12 × 1 mm disc BCZT sample or polystyrene sample (as a control) was inserted. Each sample was seeded with 1 × 10^4 cells, and the samples were incubated at 37°C and 5% CO_2 for 30 min.

Cytotoxicity and morphology were analyzed with FDA (fluorescein diacetate)/PI (propidium iodide) dual staining (FDA of 10 μg/mL in phosphate-buffered saline [PBS], Invitrogen GmbH, Karlsruhe, Germany; PI of 50 μg/mL in PBS, Invitrogen GmbH, Karlsruhe, Germany). Media were removed after 24 hr and samples were stained for 20 min. After rinsing with PBS, the samples were inspected with an inverse microscope (Axioskop, Carl Zeiss AG, Oberkochen, Germany). Polystyrene and BCZT samples were compared for cell proliferation. Cell proliferation was determined by the number of live cells after 1, 3, 7, and 10 days with Scepter™ 2.0 Cell Counter (Merck KGaA, Darmstadt, Germany). The cells were detached at specific time points with Accutase (Accutase© Innovative Cell Technologies Inc., San Diego, CA), washed with PBS, and counted. Cell viability was determined from the activity of mitochondrial dehydrogenase using the WST-1 Cell Proliferation Assay (Roche Diagnostics GmbH, Mannheim, Germany).

All cell testing measurements were performed at least five times and expressed as mean and *SD*. The BiAs software (BiAs 11.08, epsilon-Verlag, Frankfurt, Germany) was used for analysis. The Kruskal–Wallis test was employed to assess the statistical significance of the data. The probability values of $p < 0.05$ were considered to be statistically significant (McDonald, 2014).

3 | RESULTS

3.1 | Structural analysis

Figure 1 displays the XRD patterns of sintered powder BCZT Series 1 and 2. The absence of secondary phases in the diffractograms shows that both Series 1 and 2 are phase pure. In addition, peak splitting is observed for the (200) and (222) reflections at 45° and 83°, showing that both tetragonal and rhombohedral crystal structures are present. This confirms the composition as being located in the morphotropic phase boundary region.

3.2 | Microstructural analysis

Figure 2 shows the representative SEM images of both series of sintered BCZT samples and the average grain sizes are provided in Table 1

together with the average densities. It can be seen that Series 1 has significantly smaller grains than Series 2 and a higher average density.

3.3 | Characterization of the piezoelectric properties

The piezoelectric coefficient, d_{33}, is the amount of induced charge per unit of applied mechanical stress. For a piezoelectric ceramic to exhibit a macroscopic piezoelectric response, the material must be electrically poled at first. This is because the electric dipoles are aligned with each other within a domain, but each domain is spatially oriented in a random fashion cancelling out the overall piezoelectric characteristic. The application of a sufficiently high electric field will cause the dipoles to align with the direction of the applied electric field and a macroscopic piezoelectric coefficient can be measured. A visual illustration of this process is given in Figure 3, which shows the d_{33} hysteresis loop of BCZT Series 1 ceramics during the initial polarization step. At point A (d_{33} = 0), the piezoelectric material is unpoled and contains randomly oriented domains that form a net zero piezoelectric coefficient. As the electric field is increased up to the coercive field, E_c, there is a sudden increase in d_{33} as the domains align along the direction of the applied electric field. At point B (d_{33s} > 0), a saturation state is reached. As the electric field is reduced again, some domains move out of alignment, but the material does not return to its original state. Instead it maintains a remanent alignment of domains at point C (d_{33r} > 0) upon complete removal of the electric field. This remanent piezoelectric coefficient, d_{33r}, is important as it demonstrates the amount of charge that can be retained without electric field application and therefore be applied to surrounding human cells when used in a biological environment. Upon further application of a negative electric field, domains within the material switch their direction, allowing the material to express a surface charge and with this a piezoelectric coefficient of opposite polarity.

Figure 4 shows the d_{33} hysteresis loops for Series 1 and 2 in comparison. Although Series 1 exhibits significantly higher piezoelectric responses while high electric fields are applied, both series demonstrate similarly high remanent d_{33r} values of ≈ 280 pC/N.

3.4 | Cell studies

The cell viability of primary HOBs and primary HUVECs on BCZT and a polystyrene control group was investigated by FDA/PI dual staining,

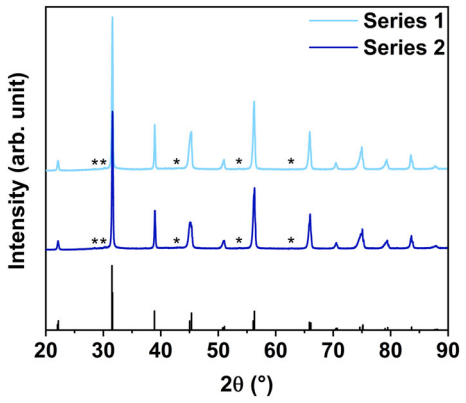

FIGURE 1 XRD patterns of BCZT–Series 1 and 2, synthesized using $BaCO_3$ precursor powders of purity level ≥ 99% and ≥ 99.98%, respectively. The asterisks (*) mark contributions from Cu Kβ1 and W Lα1 radiation from the XRD measurement. The reference diffractogram, PDF 00-065-0109, used for the phase purity analysis is shown

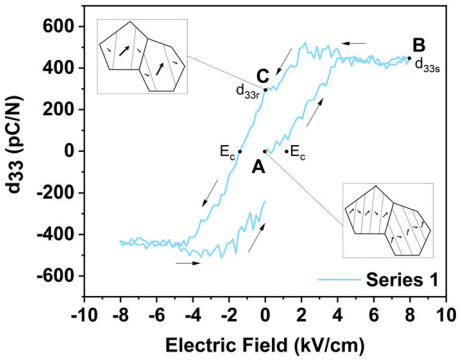

FIGURE 3 d_{33} hysteresis loop of BCZT Series 1, during the initial polarization step. The d_{33} increases from a value of zero with the application of electric field. Arrows denote the direction of electric field application

TABLE 1 Average grain sizes and densities of BCZT Series 1 and 2, synthesized using $BaCO_3$ ≥99% and ≥99.98% precursor powders, respectively

Sample	Number of samples	Average grain size (μm)	Average density (g/cm^3)
Series 1	88	10 ± 2	6.0 ± 0.3
Series 2	23	35 ± 8	5.6 ± 0.3

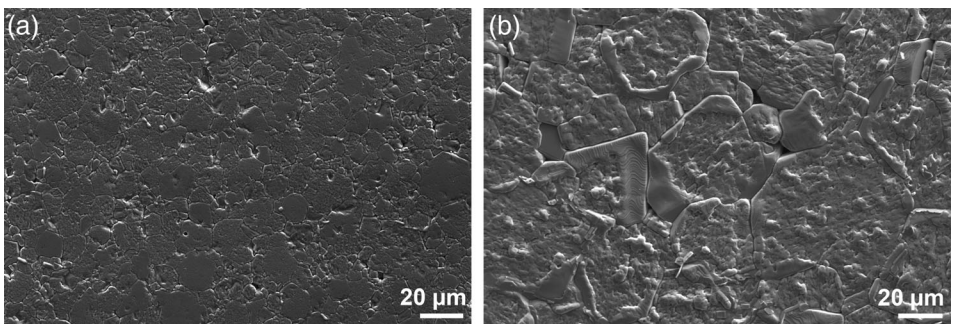

FIGURE 2 SEM micrographs of polished and etched BCZT (a) Series 1, synthesized using $BaCO_3$ precursor powder of purity level ≥ 99%, and (b) Series 2, synthesized using $BaCO_3$ precursor powder of purity level ≥ 99.98%

as displayed in Figure 5. Viable cells are stained green and dead cells are stained red. As shown in Figure 5, vital and adjacent cells with well-spread filopodiae were observed on both BCZT and the polystyrene control group after 24 hr in cell culture. In general, significantly more vital HOBs were observed on both materials than HUVECs and an increased number of viable HOB cells are observed on BCZT than on the polystyrene control group.

Cell proliferation was observed on both BCZT and the polystyrene control group, as shown in Figure 6. A constant proliferation of HUVECs and HOBs on BCZT was observed from Days 1 to 7. On Day 10, the cell count on BCZT decreased to 3.4×10^4 for HUVECs and 3.8×10^4 for HOBs. Constant proliferation of HUVECs and HOBs was observed on the polystyrene control group over the entire 10-day period. The HUVECs cell culture showed better statistically significant proliferation rates on BCZT from Days 1 to 7, as shown in Table 2 and Figure 6. The cell culture of HOBs, however, reveals statistically significant results on Days 7 and 10, as shown in Table 2 and Figure 6.

Cell viability studies performed using a WST assay show that a higher number of living cells were detected on the BCZT ceramics at all time points during the 10-day period as compared to the control group for both cell lines. This is evident in Figure 7, which shows the percentage of viable HUVECs and HOBs on BCZT in comparison to the polystyrene control group over the 10-day period.

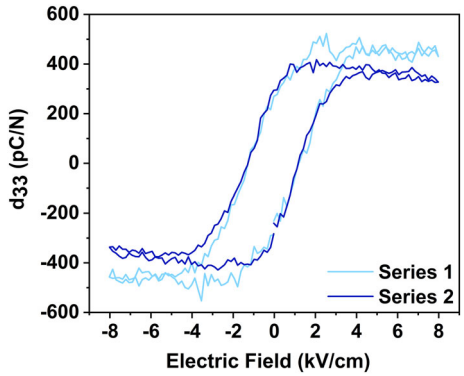

FIGURE 4 d_{33} hysteresis loops of BCZT Series 1 and 2 after polarization

Detailed progressions of the cell viability during the testing period for HUVECs and HOBs on the BCZT ceramics and polystyrene control group are presented in Figure 8, with a higher absorbance indicating a higher activity of mitochondrial dehydrogenase and amount of viable metabolically active cells. A greater proportion of HUVECs were viable on the BCZT ceramics as compared to the polystyrene control group for all days. A similar trend is seen for the HOBs, with the exception on Day 7, which shows a greater proportion of viable cells on the polystyrene samples. This is likely due to cell overcrowding limiting growth.

3.5 | Surface properties

Surface morphologies of BCZT and polystyrene samples as prepared for cell testing are shown in Figure 9. These images show that the BCZT ceramics, prepared by grinding with SiC paper, are rougher than the as-received polystyrene samples. The surface roughness, R_a, for BCZT was determined as 0.840 μm and <0.001 μm for the polystyrene control group. Deionized water contact angle measurements were performed on BCZT and polystyrene. A greater wettability of BCZT than polystyrene was observed, with BCZT surfaces showing

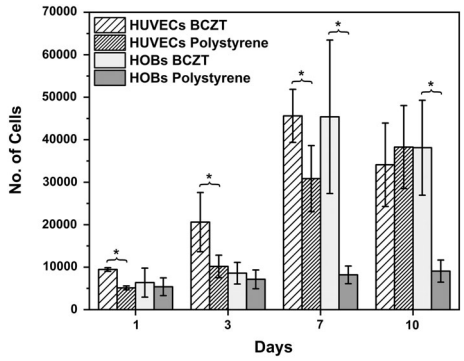

FIGURE 6 Proliferation of HUVECs and HOBs on BCZT and the polystyrene control group during a 10-day period. Statistically significant results ($p < 0.05$) are marked with an asterisk (*). Significantly higher cell numbers were observed on Days 1, 3, and 7 on BCZT as compared to the polystyrene control group for the HUVEC cell line, and on Days 7 and 10 for the HOB cell line

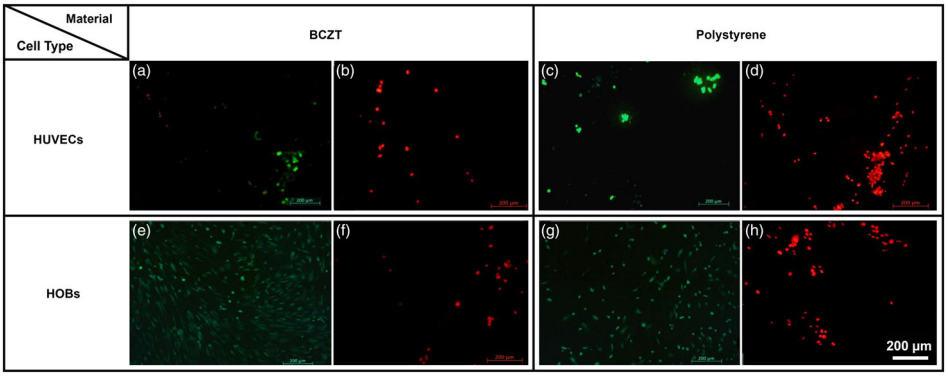

FIGURE 5 FDA/PI-viability staining of HUVECs (a–d) and HOBs (e–h) after 24 hr of cell culture on BCZT (a,b,e,f) and polystyrene (c,d,g,h). Viable cells are stained green and dead cells red

TABLE 2 Counted cell numbers at given time points

HUVECs				
	Day 1	**Day 3**	**Day 7**	**Day 10**
BCZT	9,457 ± 423	20,608 ± 6,963	45,620 ± 6,254	34,110 ± 9,822
Polystyrene	5,126 ± 461	10,175 ± 2,659	30,840 ± 7,786	38,270 ± 9,771
p	0.008*	0.016*	0.032*	0.690
HOBs				
	Day 1	**Day 3**	**Day 7**	**Day 10**
BCZT	6,368 ± 3,414	8,582 ± 2,538	45,400 ± 18,062	38,120 ± 11,179
Polystyrene	5,388 ± 2090	7,138 ± 2,203	8,200 ± 2083	9,072 ± 2,605
p	0.690	0.690	0.008*	0.008*

Note: BCZT showed highest proliferation. Statistically significant differences ($p < 0.05$) in proliferation are marked with an asterisk (*).

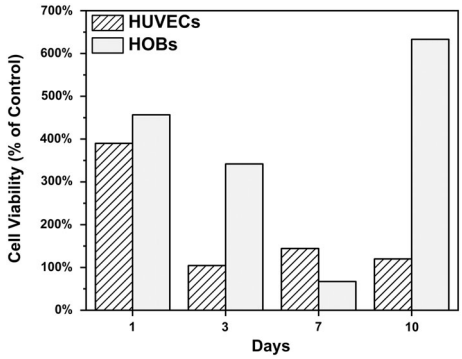

FIGURE 7 The relative amount of viable cells observed on BCZT as compared to polystyrene

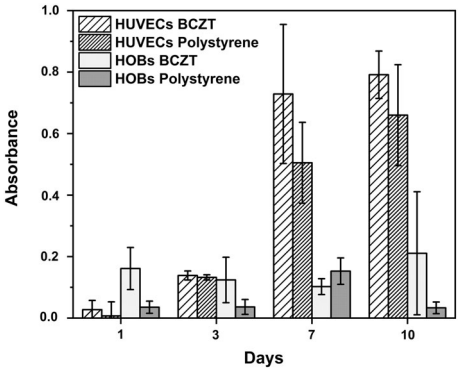

FIGURE 8 Absorbance of mitochondrial dehydrogenase activity on BCZT and polystyrene over a 10-day period

contact angles of 41.2 ± 3.9° as compared to contact angles of 87.6 ± 1.6° for polystyrene surfaces.

4 | DISCUSSION

4.1 | Grain size dependency of the piezoelectric response

The piezoelectric performance of BT-based ceramics is influenced by the microstructure and especially by the size of the grains (Arlt, 1990). Tailoring of the grain size distribution can as such be used as a tool to optimize the piezoelectric response. This is of utmost interest when piezoelectric materials are used *in vivo* as material optimization through chemical doping is restricted to the usage of non-toxic elements.

In the present study, two $BaCO_3$ precursor powders with different levels of purity were used, resulting in significantly different grain sizes of the two BCZT series. It has been reported for the $PbTiO_3$ system that minor cation non-stoichiometry can affect the microstructure due to alterations in defect chemistry and mass transport mechanisms. Although A-site deficiency leads to submicron-sized grains, B-site deficiency causes grain growth and grains become approximately two orders of magnitude larger in size (Selbach, Tybell, Einarsrud, & Grande, 2011). Parallels in behavior to the $PbTiO_3$ system can be observed in the present BCZT composition. Series 1 synthesized using $BaCO_3$ with purity ≥99% exhibits similar behavior as the A-site-deficient $PbTiO_3$, and Series 2 synthesized using $BaCO_3$ with purity ≥99.98% exhibits significantly larger grains consistent with the grain growth behavior observed in B-site deficient $PbTiO_3$ (Selbach et al., 2011). The slight variations in chemical composition introduced this way were sufficient to alter the sintering behavior leading to different grain microstructures.

Figure 4 highlights the influence of the microstructure variations on the piezoelectric performance. The figure of merit in this study is the remanent piezoelectric coefficient, d_{33r}, that is retained without the application of an external electric field. It determines the amount of charge the piezoelectric ceramics are able to supply to surrounding cells when used as a load-bearing implant. High remanent d_{33r} values of approximately 280 pC/N were obtained for both Series 1 and 2. In contrast to the values obtained under electric field application, no influence of the grain size is observed for the remanent state. This can be attributed to the inherent electrical "softness" of $BaTiO_3$-based materials. This is reflected in strong domain switching and development of high piezoelectric response under electric field application, but as well a strong relaxation of the aligned domain structure and a

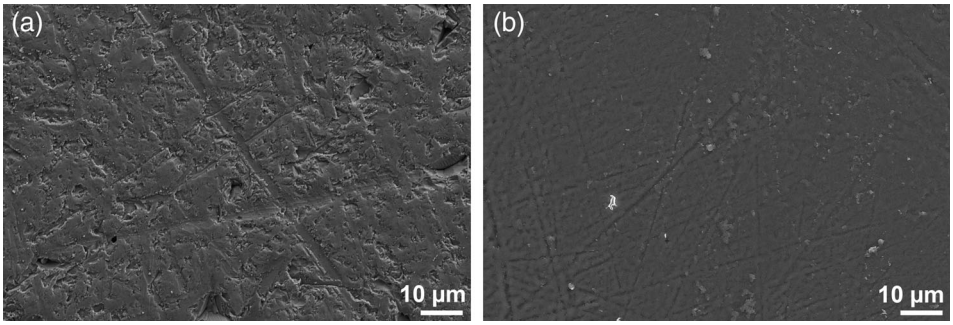

FIGURE 9 SEM micrographs of (a) BCZT surface grinded with 1200 grit SiC paper, and (b) as-received polystyrene surface, reflecting the surface roughness as present during the cell tests

corresponding reduction in response, when the electric field is reduced (Ehmke, Glaum, Hoffman, Blendell, & Bowman, 2013a; Ehmke, Glaum, Hoffman, Blendell, & Bowman, 2013b). Although the exact influence of grain size on the piezoelectric behavior of BCZT is unascertained, there are indications that there is a positive correlation between enhanced piezoelectric performance and the movement of 90° domain walls in larger grains (Arlt, 1990; Ghayour & Abdellahi, 2016). The change in mechanical constraints as imposed by a variation in average grain size does not overrule the electrical "softness" for the composition investigated in the present study. However, the grain size might take a more determining role for single phase compositions, as their piezoelectric response is less sensitive to changes in the electric field. This suggests that the piezoelectric response and, therefore, the amount of charge that can be supplied to surrounding cells may be tuned and optimized by modification of the grain size, thus removing the need for toxic elemental additives.

The density of a ceramic can influence piezoelectric performance. Higher piezoelectric performances are expected of high-density samples due to the absence of lower permittivity pores. However, it is expected that grain size is the dominant factor affecting the piezoelectric performance in this study. Despite a difference in densities for Series 1 and 2 of 6.0 g/cm^3 and 5.6 g/cm^3, it is shown that the density variation is not significant enough to affect the remanent piezoelectric state, as shown in Figure 4.

4.2 | The influence of surface properties on the cell response

It is well understood that the surface properties of an implant can affect the biological response. This has led to developments in implant surface designs, where factors such as surface roughness and wettability are considered. In the present study, the cell responses to the presence of the piezoelectric ceramics were compared to a control group, where polystyrene samples served as the substrates.

Surface wettability is one factor that can affect the biological response with respect to cell adhesion and spreading. Studies suggest that moderate contact angles of approximately 60° enhance osteoblast adhesion (Lavenus et al., 2011; Vandrovcová & Bačáková, 2011). As such, the greater wettability of the present BCZT ceramics compared to the polystyrene samples may have enhanced cell adhesion and spreading, contributing to the larger number of osteoblast cells and endothelial cells measured on the BCZT surfaces at the different time points of the cell proliferation tests, as shown in Figure 6.

Due to the nature of the sample preparation routine used, the present BCZT ceramics exhibited a significantly higher surface roughness than the polystyrene control samples (0.840 μm for the ceramics compared to <0.001 μm for the control). Roughness at the nano-, micro-, and macroscale each can have an influence on cell adhesion, spreading, and proliferation (Andrukhov et al., 2016; Gittens et al., 2013; Lavenus et al., 2011; Nishimoto et al., 2008; Samavedi, Whittington, & Goldstein, 2013; Vandrovcová & Bačáková, 2011). Enhanced cell adhesion of osteoblasts has been observed for surface roughnesses of approximately 1 μm, as compared to smoother surfaces (Andrukhov et al., 2016; Nishimoto et al., 2008; Vandrovcová & Bačáková, 2011). This indicates that the higher surface roughness of the BCZT samples may be one reason for the enhanced cell attachment as compared to the smooth surfaces of the polystyrene control group.

The intrinsic microstructure of ceramics is determined by their grain morphology (Figure 2). The grain size and shape are not expected to be critical factors for the surface properties in the current work, as the surface features exposed to the cells were determined by the grinding process (Figure 9). Furthermore, the BCZT bulk ceramic samples used for cell proliferation and viability testing were not electrically polarized. The domain structure in individual grains was therefore random (Point A in Figure 3), and it can be expected that individual grains were not electrically distinguishable to the osteoblast or endothelial cells.

However, to maximize the stimulating effect of the piezoelectrically generated charges in bone replacement applications, electrically poled materials must be used. As every grain has a different orientation of the crystallographic axis with respect to the surface of the sample, the surface charge developed under mechanical load will vary spatially from grain to grain as well as within one grain from domain to domain. Although grain to grain variations occur on a length scale from about 1–100 μm, variations on the domain scale are expected in the range of 10–500 nm with domain size becoming smaller as the grain size decreases (Tan et al., 2015). This highlights that even though the macroscopic remanent piezoelectric coefficient was found to be independent of the grain size in the present system, grain size and domain size are expected to have profound influence on the local cell responses.

5 | CONCLUSIONS

BCZT ceramics were synthesized via solid-state synthesis, and the piezoelectric performance and compatibility with human osteoblast and endothelial cells were investigated. Cell studies demonstrating elevated

cell proliferation and viability results for BCZT as compared to a polystyrene control group show the possible encouragement of cell activity. Due to good piezoelectric performance and compatibility with human osteoblast and endothelial cells, BCZT demonstrates high potential as an active bone replacement material. Further studies mapping the relationship between microstructure, local piezoelectric response, and cell stimulation are in demand to be able to take advantage of the possibility to optimize the material's functionality without the need for additional doping elements.

ACKNOWLEDGMENTS

The authors acknowledge funding from The Research Council of Norway (FRINATEK Project No. 250098) as well as from the EU call H2020- MSCA-IF-2014 under grant number 655866.

ORCID

Matthias C. Wurm https://orcid.org/0000-0002-4877-0042

REFERENCES

Aleem, I. S., Aleem, I., Evaniew, N., Busse, J. W., Yaszemski, M., Agarwal, A., & Einhorn Tand Bhandari, M. (2016). Efficacy of electrical stimulators for bone healing: A meta-analysis of randomized sham-controlled trials. *Scientific Reports*, *6*, 31724.

Andrukhov, O., Huber, R., Shi, B., Berner, S., Rausch-Fan, X., Moritz, A., … Schedle, A. (2016). Proliferation, behavior, and differentiation of osteoblasts on surfaces of different microroughness. *Dental Materials*, *32*, 1374–1384.

Arlt, G. (1990). The influence of microstructure on the properties of ferroelectric ceramics. *Ferroelectrics*, *104*, 217–227.

Bai, Y., Matousek, A., Tofel, P., Bijalwan, V., Nan, B., Hughes, H., & Button, T. W. (2015). $(Ba,Ca)(Zr,Ti)O_3$ lead-free piezoelectric ceramics—The critical role of processing on properties. *Journal of the European Ceramic Society*, *35*, 3445–3456.

Ball, J. P., Mound, B. A., Nino, J. C., & Allen, J. B. (2014). Biocompatible evaluation of barium titanate foamed ceramic structures for orthopedic applications. *Journal of Biomedical Materials Research. Part A*, *102*, 2089–2095.

Baxter, F. R., Bowen, C. R., Turner, I. G., & Dent, A. C. E. (2010). Electrically active bioceramics: A review of interfacial responses. *Annals of Biomedical Engineering*, *38*, 2079–2092.

Bodhak, S., Bose, S., & Bandyopadhyay, A. (2009). Role of surface charge and wettability on early stage mineralization and bone cell–materials interactions of polarized hydroxyapatite. *Acta Biomaterialia*, *5*, 2178–2188.

Büchter, A., Wiechmann, D., Koerdt, S., Wiesmann, H. P., Piffko, J., & Meyer, U. (2005). Load-related implant reaction of mini-implants used for orthodontic anchorage. *Clinical Oral Implants Research*, *16*, 473–479.

Dergin, G., Akta, M., Gürsoy, B., Devecioglu, Y., Kürkçü, M., & Benlidayi, E. (2013). Direct current electric stimulation in implant osseointegration: An experimental animal study with sheep. *The Journal of Oral Implantology*, *39*, 671–679.

Ehmke, M. C., Glaum, J., Hoffman, M., Blendell, J. E., & Bowman, K. J. (2013a). The effect of electric poling on the performance of lead-free $(1\text{-}x)Ba(Zr_{0.2}Ti_{0.8})O_3\text{-}x(Ba_{0.7}Ca_{0.3})TiO_3$ piezoceramics. *Journal of the American Ceramic Society*, *96*, 3805–3811.

Ehmke, M. C., Glaum, J., Hoffman, M., Blendell, J. E., & Bowman, K. J. (2013b). In situ X-ray diffraction of biased ferroelastic switching in tetragonal lead-free $(1\text{-}x)Ba(Zr_{0.2}Ti_{0.8})O_3\text{-}x(Ba_{0.7}Ca_{0.3})TiO_3$ piezoelectrics. *Journal of the American Ceramic Society*, *96*, 2913–2920.

Esguerra-Arce, J., Aguilar-Castro, Y., Aperador-Chaparro, W., Ipaz-Cuastumal, L., Bolaños Pantoja, G., & Rincón-López, C. A. (2015). Tribological behavior of bone against calcium titanate coating in simulated body fluid. *Ingeniería, Investigación y Tecnología.*, *16*, 279–286.

Foulds, I. S., & Barker, A. T. (1983). Human skin battery potentials and their possible role in wound healing. *The British Journal of Dermatology*, *109*, 515–522.

Ghayour, H., & Abdellahi, M. (2016). A brief review of the effect of grain size variation on the electrical properties of $BaTiO_3$-based ceramics. *Powder Technology*, *292*, 84–93.

Gittens, R. A., Olivares-Navarrete, R., Cheng, A., Anderson, D. M., McLachlan, T., Stephan, I., … Schwarz, Z. (2013). The roles of titanium surface micro/nanotopography and wettability on the differential response of human osteoblast lineage cells. *Acta Biomaterialia*, *9*, 6268–6277.

Griffin, M., & Bayat, A. (2011). Electrical stimulation in bone healing: Critical analysis by evaluating levels of evidence. *Eplasty*, *11*, 303–353.

Hartig, M., Joos, U., & Wiesmann, H. P. (2000). Capacitively coupled electric fields accelerate proliferation of osteoblast-like primary cells and increase bone extracellular matrix formation in vitro. *European Biophysics Journal*, *29*, 499–506.

Isaacson, B. M., Brunker, L. B., Brown, A. A., Beck, J. P., Burns, G. L., & Bloebaum, R. D. (2011). An evaluation of electrical stimulation for improving periprosthetic attachment. *Journal of Biomedical Materials Research. Part B, Applied Biomaterials*, *97*, 190–200.

Kuzyk, P. R., & Schemitsch, E. H. (2009). The science of electrical stimulation therapy for fracture healing. *Indian J Orthop.*, *43*, 127–131.

Lavenus, S., Pilet, P., Guicheux, J., Weiss, P., Louarn, G., & Layrolle, P. (2011). Behaviour of mesenchymal stem cells, fibroblasts and osteoblasts on smooth surfaces. *Acta Biomaterialia*, *7*, 1525–1534.

Liu, W., & Ren, X. (2009). Large piezoelectric effect in Pb-free ceramics. *Physical Review Letters*, *103*, 1–4.

Lucksanasombool, P., Higgs, W. A. J., Higgs, R. J. E. D., & Swain, M. V. (2001). Fracture toughness of bovine bone: Influence of orientation and storage media. *Biomaterials*, *22*, 3127–3132.

Mandracci, P., Mussano, F., Rivolo, P., & Carossa, S. (2016). Surface treatments and functional coatings for biocompatibility improvement and bacterial adhesion reduction in dental implantology. *Coatings*, *6*, 7.

McDonald, J. H. (2014). *Handbook of biological statistics*. Baltimore, Maryland: Sparky House Publishing.

Meyer, U., Büchter, A., Wiesmann, H. P., Joos, U., & Jones, D. B. (2005). Basic reactions of osteoblasts on structured material surfaces. *European Cells & Materials*, *9*, 39–49.

Minary-Jolandan, M., & Yu, M. F. (2009). Nanoscale characterization of isolated individual type I collagen fibrils: Polarization and piezoelectricity. *Nanotechnology*, *20*, 085706.

Nishimoto, S. K., Nishimoto, M., Park, S. W., Lee, K. M., Kim, H. S., Koh, J. T., … Yang, T. (2008). The effect of titanium surface roughening on protein absorption, cell attachment, and cell spreading. *The International Journal of Oral & Maxillofacial Implants*, *23*, 675–680.

Öhman, C., Zwierzak, I., Baleani, M., & Viceconti, M. (2013). Human bone hardness seems to depend on tissue type but not on anatomical site in the long bones of an old subject. *Proceedings of the Institution of Mechanical Engineers. Part H*, *227*, 200–206.

Orr, A. W., Helmke, B. P., Blackman, B. R., & Schwartz, M. A. (2006). Review mechanisms of mechanotransduction. *Developmental Cell*, *10*, 11–20.

Park, J. B., Kelly, B. J., Kenner, G. H., von Recum, A. F., Grether, M. F., & Coffeen, W. W. (1981). Piezoelectric ceramic implants: in vivo results. *Journal of Biomedical Materials Research*, *15*, 103–110.

Phelps, J. B., Hubbard, G. P., Wang, X., & Agrawal, C. M. (2000). Microstructural heterogeneity and the fracture toughness of bone. *Journal of Biomedical Materials Research*, *51*, 735–741.

Prabahar, K., Ranjith, R., Srinivas, A., Kamat, S. V., Mallesham, B., Niranjani, V. L., … Das, D. (2017). Effect of deposition temperature on the microstructure, ferroelectric and mechanical properties of lead free BCZT ceramic thin films. *Ceramics International*, *43*, 5356–5361.

Rajabi, A. H., Jaffe, M., & Arinzeh, T. L. (2015). Piezoelectric materials for tissue regeneration: A review. *Acta Biomaterialia*, *24*, 12–23.

Rattanachan, S., Miyashita, Y., & Mutoh, Y. (2005). Fracture toughness of $BaTiO_3$ and $BaTiO_3$-Al_2O_3 composite under electric field. In R. C. Bradt, D. Munz, M. Sakai, & K. W. White (Eds.), *Fracture Mechanics of Ceramics* (Vol. 14, pp. 297–305). Boston: Springer.

Riddle, R. C., & Donahue, H. J. (2009). From streaming potentials to shear stress: 25 years of bone cell mechanotransduction. *Journal of Orthopaedic Research*, *27*, 143–149.

Sailaja, P., Kumar, N. P., Sowmya, N. S., James, A. R., Kumar, A., Arockiakumar, R., & Srinivas, A. (2019). Investigation of ferroelectric, piezoelectric and mechanically coupled properties of lead-free $(Ba_{0.85}Ca_{0.15})(Zr_{0.1}Ti_{0.9})O_3$ ceramics. *Advances in Applied Ceramics*, *118*, 300–307.

Saini, M., Singh, Y., Arora, P., Arora, V., & Jain, K. (2015). Implant biomaterials: A comprehensive review. *World Journal of Clinical Cases*, *3*, 52–57.

Salman, N. N., & Park, J. B. (1980). The effect of direct electrical current stimulation on the bone/porous metallic implant interface. *Biomaterials*, *1*, 209–213.

Samavedi, S., Whittington, A. R., & Goldstein, A. S. (2013). Calcium phosphate ceramics in bone tissue engineering: A review of properties and their influence on cell behavior. *Acta Biomaterialia*, *9*, 80337–88045.

Selbach, S. M., Tybell, T., Einarsrud, M. A., & Grande, T. (2011). PbO-deficient $PbTiO_3$: Mass transport, structural effects and possibility for intrinsic screening of the ferroelectric polarization. *Applied Physics Letters*, *98*, 091912.

Shrout, T. R., & Zhang, S. J. (2007). Lead-free piezoelectric ceramics: Alternatives for PZT? *Journal of Electroceramics*, *19*, 111–124.

Smeets, R., Stadlinger, B., Schwarz, F., Beck-Broichsitter, B., Jung, O., Precht, C., … Ebker, T. (2016). Impact of dental implant surface modifications on osseointegration. *BioMed Research International*, *2016*, 1–16.

Srinivas, A., Krishnaiah, R. V., Niranjani, V. L., Kamat, S. V., Karthik, T., & Asthana, S. (2015). Ferroelectric, piezoelectric and mechanical properties in lead free $(0.5)Ba(Zr_{0.2}Ti_{0.8})O_3$-$(0.5)(Ba_{0.7}Ca_{0.3})TiO_3$ electroceramics. *Ceramics International*, *41*, 1980–1985.

Tan, Y., Zhang, J., Wu, Y., Wang, C., Koval, V., Shi, B., … Yan, H. (2015). Unfolding grain size effects in barium titanate ferroelectric ceramics. *Scientific Reports*, *5*, 9953.

Tang, Y., Wu, C., Wu, Z., Hu, L., Zhang, W., & Zhao, K. (2017). Fabrication and in vitro biological properties of piezoelectric bioceramics for bone regeneration. *Scientific Reports*, *7*, 1–12.

Tofail, S. A. M., & Bauer, J. (2016). Electrically polarized biomaterials. *Advanced Materials*, *28*, 5470–5484.

Vandrovcová, M., & Bačáková, L. (2011). Adhesion, growth and differentiation of osteoblasts on surface-modified materials developed for bone implants. *Physiological Research*, *60*, 403–417.

Wiesmann, H. P., Hartig, M., Stratmann, U., Meyer, U., & Joos, U. (2001). Electrical stimulation influences mineral formation of osteoblast-like cells in vitro. *Biochimica et Biophysica Acta*, *1538*, 28–37.

Wolff, J. (1892). *Das Gesetz der Transformation der Knochen*. Berlin: Hirschwald.

Wurm, M. C., Möst, T., Bergauer, B., Rietzel, D., Neukam, F. W., Cifuentes, S. C., & Wilmowsky, C. V. (2017). In-vitro evaluation of polylactic acid (PLA) manufactured by fused deposition modeling. *Journal of Biological Engineering*, *11*, 29.

Zhang, Y., Chen, L., Zeng, J., Zhou, K., & Zhang, D. (2014). Aligned porous barium titanate/hydroxyapatite composites with high piezoelectric coefficients for bone tissue engineering. *Materials Science and Engineering: C*, *39*, 143–149.

Zhang, Y., Glaum, J., Groh, C., Ehmke, M. C., Blendell, J. E., Bowman, K. J., & Hoffman, M. J. (2014). Correlation between piezoelectric properties and phase coexistence in $(Ba,Ca)(Ti,Zr)O_3$ ceramics. *Journal of the American Ceramic Society*, *97*, 2885–2891.

Zigman, T., Davila, S., Dobric, I., Antoljak, T., Augustin, G., Rajacic, D., … Ehrenfreund, T. (2013). Intraoperative measurement of bone electrical potential: A piece in the puzzle of understanding fracture healing. *Injury*, *44*, S16–S19.

Zioupos, P., & Currey, J. D. (1998). Changes in the stiffness, strength, and toughness of human cortical bone with age. *Bone*, *22*, 57–66.

How to cite this article: Poon KK, Matthias C. Wurm, Evans DM, Einarsrud M-A, Lutz R, Glaum J. Biocompatibility of $(Ba,Ca)(Zr,Ti)O_3$ piezoelectric ceramics for bone replacement materials. *J Biomed Mater Res*. 2020;108B: 1295–1303. https://doi.org/10.1002/jbm.b.34477